

BNL--42974

DE89 016410

BNL-42974

CONF-8906194--1

Hypernuclear physics with the ( $\pi^+$ ,  $K^+$ ) reaction

An invited paper presented by

R.E. CHRIEN

Received by OSTI

AUG 1 4 1989

at

International Meeting on Physics at KAON

Bad Honnef, F.R. Germany

June 7-9, 1989

D. J. Millener and R. E. Chrien

Physics Department  
Brookhaven National Laboratory  
Upton, New York 11973

**DISCLAIMER**

This report was prepared as an account of work sponsored by an agency of the United States Government. Neither the United States Government nor any agency thereof, nor any of their employees, makes any warranty, express or implied, or assumes any legal liability or responsibility for the accuracy, completeness, or usefulness of any information, apparatus, product, or process disclosed, or represents that its use would not infringe privately owned rights. Reference herein to any specific commercial product, process, or service by trade name, trademark, manufacturer, or otherwise does not necessarily constitute or imply its endorsement, recommendation, or favoring by the United States Government or any agency thereof. The views and opinions of authors expressed herein do not necessarily state or reflect those of the United States Government or any agency thereof.

---

This manuscript has been authored under contract number DE-AC02-76CH00016 with the U.S. Department of Energy. Accordingly, the U.S. Government retains a non-exclusive, royalty-free license to publish or reproduce the published form of this contribution, or allow others to do so, for U.S. Government purposes.

DISTRIBUTION OF THIS DOCUMENT IS UNLIMITED

MASTER

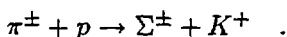
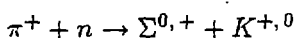
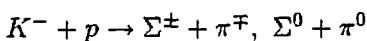
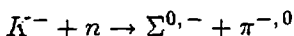
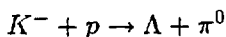
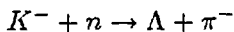
## I. INTRODUCTORY BACKGROUND

The study of hypernuclei affords unique insights into the nature of hadronic forces beyond those obtainable from ordinary nuclear physics research. A hypernucleus consists of one or more hyperons bound to a nuclear core. In the SU(3) classification, the  $\Lambda$ ,  $\Sigma$ , and  $\Xi$  hyperons occupy the same octet representation of spin-parity  $1/2^+$  baryons as the neutron and proton, the familiar constituents of ordinary nuclei. The  $\Lambda$  and  $\Sigma$  possess strangeness  $S = -1$  and isotopic spin  $I = 0, 1$ , respectively, while the  $\Xi$  has  $S = -2$ ,  $I = 1/2$ . In the underlying quark picture, the  $\Lambda$  and  $\Sigma$  have the flavor structure  $s(ud)_{I=0,1}$ , compared to the combination  $uud$  for the proton. The strange quark,  $s$ , carries the strangeness quantum number  $S = -1$ , which makes it distinguishable from the  $S = 0$   $u$  and  $d$  quarks. The lowest-lying hyperon is the  $\Lambda$ , with a mass of  $1115.6 \text{ MeV}/c^2$ , some  $177 \text{ MeV}/c^2$  heavier than the proton. The study of the behavior of a hyperon embedded in the nuclear medium, through the theoretical analysis of level spectra, sheds light on the nature of the hyperon-nucleon ( $YN$ ) effective interaction, i.e. on the role of the strange quark in strong interactions.

A single  $\Lambda$  behaves essentially as a distinguishable particle in the nucleus: there are no discontinuities in the binding energy  $B_\Lambda$  as a function of  $A$ , a signal of shell effects in ordinary nuclei. This property of the  $\Lambda$  implies additional dynamical symmetries for hypernuclear states that are not allowed for ordinary nuclei because of the Pauli principle. The  $\Lambda$  provides a superb example of single-particle structure in a many-body system. Deeply bound nucleon-hole states are very broad, a reflection of the large spreading width  $\Gamma_\dagger$  caused by admixtures with more complicated configurations. For the  $\Lambda$ , even for  $s$ -states in heavy system,  $\Gamma_\dagger$  is rather small, which indicates the rather weak  $\Lambda N$  residual interaction. The existence of a well-defined set of single particle states of different orbital angular momentum  $\ell$  in a given hypernucleus enables one to extract information on the

well depth, geometrical shape, and effective mass, all of which characterize the  $\Lambda$ -nucleus potential.

The principal production mechanisms for hypernuclei are strangeness exchange and associated production, corresponding to the elementary processes



Of these reactions, only those involving charged mesons in the exit channel have been studied extensively. In the case of nuclear species, the  $n$ ,  $p$  above are replaced with the corresponding target nuclide.

The characteristic differences between the  $(K, \pi)$  and  $(\pi, K)$  production modes have been discussed by Dover, Ludeking & Walker<sup>1</sup> and by Bandō & Motoba,<sup>2,3</sup> among others. The  $(K, \pi)$  reaction at small angles is a process with small momentum transfer  $q$ . It preferentially populates "substitutional" hypernuclear states, i.e. those states in which a nucleon in a shell model orbit with orbital angular momentum  $\ell$  and total spin  $j$  is replaced by a  $\Lambda$  particle in the same orbit  $(\ell, j)$ . This transition is characterized by an orbital angular momentum transfer of  $\Delta L = 0$ . For the  $(K, \pi)$  reaction, there exists a "magic momentum," i.e. a value of lab kaon momentum  $p_K$  for which  $q$  vanishes at  $\theta = 0^\circ$ . This corresponds to  $p_K = 530 \text{ MeV}/c$  for  $\Lambda$  and  $290 \text{ MeV}/c$  for  $\Sigma^0$  production. Note that  $q$  at  $\theta = 0^\circ$  remains less than  $100 \text{ MeV}/c$  for  $p_K \leq 800 \text{ MeV}/c$ . At or near the magic momentum, the substitutional transitions with  $\Delta L = 0$  are particularly enhanced with

respect to those for which  $\Delta L \neq 0$ . The  $\Lambda$  hypernuclear states populated in  $\Delta L = 0$  transitions tend to occur near, or above, zero  $\Lambda$  binding. The  $(K^-, \pi^-)$  process involves strong absorption of both the incoming and outgoing waves and consequently is localized in the nuclear periphery.

For the associated production  $(\pi^+, K^+)$  reaction, there is no magic momentum, and  $q \geq 350$  MeV/c at the elementary cross section maximum near  $p_K \approx 1050$  MeV/c. The formation of high spin states is favored by the form factor of the  $(\pi^+, K^+)$  reaction. Furthermore, because of the long mean free path in nuclear matter for the  $K^+$ , the distortion for the outgoing wave is reduced; the reaction is less peripheral in nature. Figure 1 nicely illustrates the comparison between  $(K^-, \pi^-)$  and  $(\pi^+, K^+)$  strength distributions. One sees the complementarity of these two reactions in exciting the low and high spin parts, respectively, of the hypernuclear spectrum.

The associated production of  $\Lambda$  hypernuclei by the  $(\pi^+, K^+)$  reaction was first studied theoretically by Dover et al.<sup>1</sup> and demonstrated in experiments carried on at the Moby Dick spectrometer at the AGS.<sup>4-7</sup>

For  $(\pi^+, K^+)$  reaction studies, the restrictions imposed by the use of beam separators and decay backgrounds are not so severe. The principal problem in such studies is the relatively smaller cross sections for  $(\pi^+, K^+)$  as compared to the  $(K^-, \pi^-)$  production of substitutional states. To compensate for the lower cross section, incident beam intensities of up to  $10^7$  pions per second have been used in the Moby Dick configuration. The problem then reduces to the difficulties of handling particle intensities in that range. The rather significant contamination of pion beams with a positron component presents further difficulties with such beams, as it becomes difficult to separate positrons and pions at momenta of 1 GeV/c and above.

The experimental arrangement for  $(\pi^+, K^+)$  differs in several respects from the corresponding  $(K^-, \pi^-)$  reactions. The elementary  $(\pi, K)$  cross section has a maximum near  $p_\pi = 1050 \text{ MeV}/c$ , which is at the upper limit for the LESB-1 line, and well above the  $700 - 800 \text{ MeV}/c$  usually chosen for the strangeness-exchanging  $(K^-, \pi^-)$  reaction. The roles of the kaon and pion spectrometers are interchanged, and the beam separator is tuned for pion transmission. Cerenkov counters are added after the target to veto pions in the rear spectrometer.

The cross sections obtained by Milner et al.<sup>4</sup> for the  $1^-$  ground state and the  $0^+, 2^+, 2^+$  excited state multiplet in  ${}^{12}_\Lambda\text{C}$  near  $11 \text{ MeV}$  agree well with the DWBA calculated cross sections, after Fermi motion is folded in and realistic optical model parameters for the  $\pi^+$  and  $K^+$  distorted waves are used. It is interesting to observe that the lower cross sections characteristic of the  $(\pi^+, K^+)$  reaction on light hypernuclei, compared to those for  $(K^-, \pi^-)$ , are more than compensated by the increased particle flux available for pions as compared to kaons.

For hypernuclei beyond the  $p$ -shell,  $(K, \pi)$  reactions become less effective in populating bound states of hypernuclei because of the increasingly higher angular momentum of the valence shell neutrons. The coupling of the  $\Lambda$  to the high-spin neutron hole produces an advantageous momentum matching for the  $(\pi^+, K^+)$  reaction, as discussed by a number of authors. The high spin selectivity preferentially highlights a series of states in which the  $\Lambda$ -shell model orbitals ( $s, p, d, f \dots$ ) couple to the valence neutron hole. The lack of spin-dependence in the  $\Lambda$  nuclear interaction produces a set of regularly spaced, narrow, single particle excitations that dominate over other more complicated particle-hole excitations. This strikingly simple sequence of levels was illustrated by Bandō & Motoba<sup>2</sup> for  ${}^{56}_\Lambda\text{Fe}$  (see Fig. 1). The cross sections can be calculated by a distorted-wave impulse approximation (DWIA) and are measurable, even for deeply-lying orbitals of heavy hypernuclei. In the

second ( $\pi^+$ ,  $K^+$ ) experiment,<sup>5-7</sup> eight targets were examined at  $\theta = 10^\circ$ :  $^9\text{Be}$ ,  $^{12}\text{C}$ ,  $\text{H}_2\text{O}$ ,  $\text{Si}$ ,  $^{13}\text{C}$ ,  $^{51}\text{V}$ ,  $\text{Ca}$ , and  $^{89}\text{Y}$ . For the latter four targets, beam particle intensities up to  $10^7$  pions per second were found usable with targets of reasonable size, namely  $2 - 4 \text{ g/cm}^2$ . The ( $\pi^+$ ,  $K^+$ ) spectra are observable over an irreducible background level of less than  $100 \text{ n.b./sr/MeV}$ , which allows a clear observation of the  $s_\Lambda$  ground state peak for  $^{89}_\Lambda\text{Y}$ , expected to be populated at a level of  $0.5 \mu\text{b/sr}$ . Figure 2 shows the data obtained for  $^{89}_\Lambda\text{Y}$ .

These two experiments have demonstrated that the ( $\pi$ ,  $K$ ) reaction is the method of choice for producing all but the lightest hypernuclei, preferable to ( $K$ ,  $\pi$ ) for directly accessing deeply lying hypernuclear states. They have made possible the interpretation of  $\Lambda$  single particle spectra in terms of the  $\Lambda$ -nucleus mean field.

Recently, through the ( $\pi^+$ ,  $K^+$ ) studies at Brookhaven National Laboratory, it has become possible to track the evolution of  $\Lambda$  binding energies (ground and excited states) as a function of  $A$ , up to  $A \approx 90$ . The results for  $s_\Lambda$ ,  $p_\Lambda$ ,  $d_\Lambda$  and  $f_\Lambda$  single-particle binding energies, as obtained from ( $\pi^+$ ,  $K^+$ ), ( $K^-$ ,  $\pi^-$ ) and emulsion measurements, are plotted in Fig. 3, taken from Millener et al.<sup>8</sup> The  $A$  dependence of the  $\Lambda$  level spacings enables us to constrain the geometry of the  $\Lambda$ -nucleus potential and also the well depth  $D_\Lambda$ .

A useful description of the data can be obtained in the Skyrme-Hartree-Fock approach, first used for hypernuclei by Rayet. Here, the nonlocality of the  $\Lambda$ -nucleus potential is parameterized in terms of an effective mass  $m_\Lambda^*(r)$ . The equivalent energy-dependent local potential  $V_\Lambda(r, E)$  is of the form:

$$\begin{aligned}
 V_\Lambda(r, E) &= \frac{m_\Lambda^*(r)}{m_\Lambda} U(r) + \left(1 - \frac{m_\Lambda^*(r)}{m_\Lambda}\right) E \\
 U(r) &= t_0 \rho(r) + \frac{3}{8} t_3 \rho^2(r) + \frac{1}{4} (t_1 + t_2) T(r) \\
 T(r) &= \frac{3}{5} \left(\frac{3\pi^2}{2}\right)^{2/3} \rho^{5/3}(r) \\
 \frac{\hbar^2}{2m_\Lambda^*(r)} &= \frac{\hbar^2}{2m_\Lambda} + \frac{1}{4} (t_1 + t_2) \rho(r) .
 \end{aligned} \tag{1}$$

The  $t_3\rho^2(r)$  term can be used to adjust the potential radius, while the  $(1 - m_\Lambda^*/m_\Lambda)E$  term serves to spread out the single particle levels; this enables one simultaneously to fit the spectra of light ( ${}^{16}_\Lambda\text{O}$ ) and heavy ( ${}^{89}_\Lambda\text{Y}$ ) systems. The choice

$$\begin{aligned} t_0 &= -402.6 \text{ MeV} \cdot \text{fm}^3 \\ t_1 + t_2 &= 103.4 \text{ MeV} \cdot \text{fm}^5 \\ t_3 &= 3394.6 \text{ MeV} \cdot \text{fm}^6 \end{aligned} \quad (2)$$

leads to the fit displayed in Fig. 3. These values correspond to

$$\frac{m_\Lambda^*(r=0)}{m_\Lambda} \approx 0.8 \quad (3)$$

$$D_\Lambda \approx 27.5 \text{ MeV}$$

The calculations of Yamamoto et al.,<sup>9</sup> which incorporate self-consistency and rearrangement energies (omitted by Millener et al.<sup>8</sup>), are consistent with the need for a strong repulsive  $t_3\rho^2(r)$  term and a modest degree of nonlocality ( $m_\Lambda^*(0)/m_\Lambda \approx 0.8$ ).

A strong  $t_3\rho^2(r)$  term is also required to fit nucleon binding energies. However, within the Skyrme-Hartree-Fock model, one cannot simultaneously describe nucleon levels near the Fermi surface (which requires  $m_N^*(0)/m_N \approx 1$ ) and deeply bound levels (for which  $m_N^*(0)/m_N \approx 1/2$ ). For the  $\Lambda$ , on the other hand, a description of all levels is possible with a single  $m_\Lambda^*(0)/m_\Lambda$ .

The  $\Lambda$  behaves as a distinguishable particle in the nucleus. Unlike deeply bound nucleon-hole states, which are very broad, deeply bound  $\Lambda$  single particle states remain well defined. The possibility that strange quarks in the nucleus are partially deconfined is an intriguing one, but the signature of this effect in the  $\Lambda$  binding energies is likely to

be subtle and easily masked by the complicated (but conventional) dynamics of density-dependent interactions.

An excellent example of the complementarity of the  $(K^-, \pi^-)$  and  $(\pi^+, K^+)$  reactions in investigation of hypernuclear structure is afforded by the case of  ${}^9_{\Lambda}\text{Be}$ . The  ${}^9\text{Be}(K^-, \pi^-){}^9_{\Lambda}\text{Be}$  reaction at forward angles has been investigated at CERN. The spectrum at 720 MeV/c is shown in Fig. 4, along with the excitation function of the  ${}^9\text{Be}(\pi^+, K^+){}^9_{\Lambda}\text{Be}$  reaction at 1.05 GeV/c. The structure of  ${}^9_{\Lambda}\text{Be}$  was discussed in the shell model framework by Dalitz & Gal<sup>10</sup> and later by Auerbach et al.<sup>11</sup> The cluster model for  ${}^9_{\Lambda}\text{Be}$  has been extensively developed.

The essential features of the  ${}^9_{\Lambda}\text{Be}$  spectrum can be seen in a coupling scheme defined by  $J = L + s_{\Lambda}$ ,  $L = J_c + \ell_{\Lambda}$ , where  $J_c$  is the spin of the nuclear core. For an interaction independent of the  $\Lambda$  spin  $s_{\Lambda}$ ,  $L$  is a good quantum number, and states with  $J = L \pm 1/2$  (for  $L \neq 0$ ) form a degenerate doublet. The structure of  ${}^9_{\Lambda}\text{Be}$  is similar to  ${}^{13}_{\Lambda}\text{C}$  in that the  $LS$  structure of the  $p^4$  core of  ${}^8\text{Be}$  with [4] and [31] symmetries resembles the [44] and [431] symmetries for  ${}^{12}\text{C}$ . The neutron pickup strength goes mostly to the  ${}^8\text{Be}$  ground state, the  $2^+$  state at 2.94 MeV, a group of states between 16 and 20 MeV and a  $3^+$  level above 19 MeV.

It is instructive to consider the  ${}^8\text{Be}(0^+, 2^+) \times p_{\Lambda}$  states in  ${}^9_{\Lambda}\text{Be}$ , in comparison with  ${}^{13}_{\Lambda}\text{C}$ . The  $0^+$  (ground state) and  $2^+$  (2.94 MeV) states in  ${}^8\text{Be}$  have almost pure [4] spatial symmetry with  $S = 0$ . Thus the states of  ${}^9_{\Lambda}\text{Be}$  can have [5] or [41] symmetry, respectively. Since the  ${}^8\text{Be}$  core is prolate while  ${}^{12}\text{C}$  is oblate, the matrix element of the quadrupole operator  $Q$  for  ${}^8\text{Be}$  is opposite in sign to that for  ${}^{12}\text{C}$ ; this implies an inverted order in  ${}^9_{\Lambda}\text{Be}$  of the  $L = 1, 2, 3$  states based on the  $2^+$  core state. There is then stronger mixing in  ${}^9_{\Lambda}\text{Be}$  than in  ${}^{13}_{\Lambda}\text{C}$  of  $L = 1$  states based on the  $0^+$  and  $2^+$  core states. For  $F^{(2)} = -3.2$  MeV, as derived earlier, this mixing is strong enough so that the eigenstate approaches the limit of good

spatial symmetry  $[[5] L = 1]$ . An important consequence is that the  ${}^9\text{Be}(K^-, \pi^-)_{\Lambda}$  cross section at  $0^\circ$ , leading to the lowest  $3/2^-$  state ( $L = 1$ ), becomes very small relative to the second  $3/2^-$  state ( $L = 1$ ), because the transition  $[41] \rightarrow [5]$  is forbidden for  $\Delta L = 0$ . The remainder of the  $\Delta L = 0$  strength is found in two states with  $T = 0, 1$ , about 12.5 MeV above the second  $3/2^-$  level. This is in excellent agreement with the  $(K^-, \pi^-)$  data shown in Fig. 4. which display two strong peaks (at 7 and 19 MeV) separated by about 12 MeV.

The simplest version of the cluster model for  ${}^9\text{Be}$ , namely  $\alpha + \alpha + \Lambda$ , does not explain the third peak at 19 MeV in the  $(K^-, \pi^-)$  spectrum of Fig. 4, since this involves a strong contribution of isospin one-core excited states of  ${}^8\text{Be}$ . The cluster model was recently extended<sup>12</sup> to include  $\alpha + \alpha^* + \Lambda$  configurations, where  $\alpha^*$  is the intrinsic excited state of the  $\alpha$  particle. The distribution of  $(K^-, \pi^-)$  strength for this model, shown in Fig. 5, is rather similar to that obtained in the shell model.

The  $(\pi^+, K^+)$  reaction, in contrast to  $(K^-, \pi^-)$  at  $0^\circ$ , favors the excitation of the higher spin states in  ${}^9\text{Be}$ . The predicted strength distribution of the  ${}^9\text{Be}(\pi^+, K^+)_{\Lambda}$  reaction at 10.5 GeV/c is shown in Fig. 5. In contrast to the  $(K^-, \pi^-)$  spectrum, one expects a measurable cross section to the "supersymmetric"  $3^-$  state near  $-B_{\Lambda} \approx 4$  MeV; these states were first discussed by Dalitz & Gal. Further, a peak near  $-B_{\Lambda} \approx 12$  MeV, corresponding to  ${}^8\text{Be}^*(2^+, 1^+, 3^+) \times s_{\Lambda}$ , should be seen in  $(\pi^+, K^+)$ , but not in  $(K^-, \pi^-)$ . The experimental  $(\pi^+, K^+)$  spectrum of Fig. 4 indicates three peaks below  $-B_{\Lambda} = 15$  MeV, consistent with dominant excitation of  $L^{\pi} = 2^+$ , ( $B_{\Lambda} = 2$  MeV),  $3^-$  ( $B_{\Lambda} = -4$  MeV) and  $2^+$  ( $B_{\Lambda} = -12$  MeV) states. The hypernucleus  ${}^9\text{Be}$  affords an excellent example of the complementary use of both  $(K^-, \pi^-)$  and  $(\pi^+, K^+)$  to obtain a more complete picture of the hypernuclear spectrum.

## II. HYPERNUCLEAR PHYSICS FOR THE FUTURE

Some possibilities for a research program with high intensity (assumed  $2 \times 10^8 \pi^+$ /sec. which is about 20 times current AGS intensities) and good resolution (possibly 100 keV, to be compared with 2 – 3 MeV at BNL) are outlined.

### 1. Spectroscopy with the $(\pi^+, K^+)$ reaction

#### (a) $\Lambda$ single-particle binding energies

As noted in the introduction, the  $(\pi^+, K^+)$  reaction at  $p_\pi \sim 1.05$  GeV/c is the optimal way to produce heavy  $\Lambda$  hypernuclei. This has been verified at Brookhaven<sup>4-7</sup> for targets up to  $A = 90$ . The presentation<sup>5</sup> of the results of a preliminary analysis of the data has produced a rash of theoretical papers.<sup>14-17</sup>

On targets with last-filled neutron orbits of high spin, the  $(\pi^+, K^+)$  spectrum is dominated by the excitation of a series of high spin  $j_N^{-1}\ell_\Lambda$  particle-hole states, as illustrated in Fig. 2 for a  $^{89}\text{Y}$  target. The energies of the  $g_{9/2}^{-1}\ell_\Lambda$  states define the binding energies of  $\Lambda$  single particle states which fit into the regular pattern shown in Fig. 3 and determine rather precisely the essential characteristics of the  $\Lambda$ -nucleus single particle potential.<sup>8</sup>

Better data for the  $f_{7/2}^{-1}\ell_\Lambda$  series states using a target with  $A \sim 50$  would be welcome; the  $^{51}\text{V}(\pi^+, K^+)^{51}\Lambda\text{V}$  data from BNL suffer from poor statistics due to limited running time. Motoba et al.<sup>14-16</sup> present theoretical spectra for a  $^{56}\text{Fe}$  target. The  $h_{11/2}^{-1}\ell_\Lambda$  series should be easily observed using any of the  $N = 82$  nuclei, all of which exhibit  $h_{11/2}$  pickup strength concentrated in a low-lying state, as a target<sup>18</sup> (e.g.  $^{136}\text{Xe}$ ,  $^{138}\text{Ba}$ ,  $^{140}\text{Ce}$ ,  $^{142}\text{Nd}$ ,  $^{144}\text{Sm}$ ).

For heavier targets the spacing of the  $\Lambda$  single-particle states decreases and good resolution is required. E.g., for  $^{208}\text{Pb}$  the  $i_{13/2}^{-1}\ell_\Lambda$  and  $h_{9/2}^{-1}\ell_\Lambda$  series are interleaved, and the strongly excited states are separated<sup>2,15</sup> by about 2 MeV.

(b)  $(\pi^+, K^+)$  cross sections

A representative sample of calculated cross sections for the production of hypernuclear states with the  $\Lambda$  in an  $s$  orbit are given in Table 1. Angular distributions for various particle-hole configurations populated in the  $^{89}\text{Y}(\pi^+, K^+)^{89}_{\Lambda}\text{Y}$  reaction are given in Table 2.

These cross sections are calculated using optical potentials derived from the elastic scattering of 800 MeV/c  $\pi^+$  and  $K^+$  on  $^{12}\text{C}$  (similar results are obtained for optical potentials derived from elastic scattering on  $^{40}\text{Ca}$ , which are preferable for calculations involving heavy nuclei) and Fermi-average elementary  $n(\pi^+, K^+)\Lambda$  cross sections. Such calculations give a good account of the Brookhaven data.

It would be useful to have measurements on pion elastic scattering at 1.05 GeV/c to improve our knowledge of the pion optical potentials which serve as input to the calculation of  $(\pi^+, K^+)$  cross sections.

(c) *Fine structure in  $(\pi^+, K^+)$  spectra*

The widths of the prominent peaks in the  $^{89}\text{Y}(\pi^+, K^+)^{89}_{\Lambda}\text{Y}$  spectra are somewhat broader than can be accounted for by the experimental resolution. There are a number of possible reasons for this.

- (i) The  $g_{9/2}^{-1}$  strength in the  $^{88}\text{Y}$  core nucleus is shared by  $4^-$  and  $5^-$  levels 233 keV apart, and the  $\Lambda$  couples to both states. For a  $^{90}\text{Zr}$  target the  $g_{9/2}^{-1}$  strength would be concentrated in a single state.
- (ii) For  $\ell_{\Lambda} \neq 0$ , there is a spin-orbit splitting for the  $\Lambda$  orbits. This splitting is known to be small but, as yet, there is no precise measurement of  $\Lambda$  spin-orbit potential.
- (iii) The simple  $j_N^{-1}j_{\Lambda}$  configurations serve as doorway states which can mix with a dense background  $\Lambda$  hypernuclear state (in analogy to an isobaric analog state which mixes with a dense background of  $T <$  states) leading to a spreading width.

(iv) The  $A \approx 90$  nuclei have low-lying  $f_{5/2}$  neutron hole states and a broad distribution of  $f$  hole strength at higher excitation energy. Hypernuclear configurations based on these states will give rise to some sharp states and a broad distribution of strength underlying the sharp states.

High resolution  $(\pi^+, K^+)$  studies could shed some light on the widths of the prominent peaks and on possible fine structure in the spectra.

(d) *Structure in light  $\Lambda$  hypernuclei*

For  $p$ -shell targets there are large  $(\pi^+, K^+)$  cross sections for  $p_N \rightarrow s_\Lambda$ ,  $\Delta L = 1$  and  $p_N \rightarrow p_\Lambda$ ,  $\Delta L = 2$  transitions to discrete states, as exemplified by the original  $^{12}\text{C}(\pi^+, K^+)^{12}_\Lambda\text{C}$  experiment.<sup>4</sup> With good resolution, there is much detailed spectroscopy which could be done on a wide range of target nuclei. The energy separations of states and their relative (and absolute)  $(\pi^+, K^+)$  cross sections would help enormously in defining the effective  $\Lambda N$  interaction. A simple example is provided by two  $2^+$  states around 11 MeV excitation energy in  $^{12}_\Lambda\text{C}$ . These states, which are predominantly mixtures of  $\Lambda$  particles in  $p_{3/2}$  and  $p_{1/2}$  orbits coupled to the  $^{11}\text{C}$   $3/2^-$  ground state are not resolved in the Brookhaven  $(\pi^+, K^+)$  experiments. However, emulsion data<sup>19</sup> shows two  $2^+$  states (and a  $0^+$  state) below the  $^{11}\text{C} + \Lambda$  threshold, separated by 750 keV and with proton decay widths of about 500 keV. The energy separation of the  $2^+$  states is clearly sensitive to the spin-orbit splitting between the  $p_{3/2}$  and  $p_{1/2}$   $\Lambda$  orbitals. Also, shell-model calculations show that the relative formation strength for the two states is a very sensitive function of the spin-orbit splitting and the detailed nature of the  $\Lambda N$  effective interaction. There are many other examples<sup>11</sup> where the energy separations and cross sections of dominantly  $p^n p_\Lambda$  configurations could be measured in  $(\pi^+, K^+)$  experiments with good resolution.

In the case of a  $\Lambda$  in an  $s$  orbit coupled to a nuclear core state with non-zero spin, all the evidence suggests that whatever spin dependence exists in the  $\Lambda N$  interaction usually

conspires to yield very small doubled splittings in the 100 keV range.<sup>20</sup> In any case, it is most often true that only one member of the doublet will be strongly populated in the  $(\pi^+, K^+)$  reaction. Nevertheless, precision measurements of the separation between states based on different nuclear core states would yield information on the  $\Lambda N$  effective interaction. To return to the case of  ${}^{12}_{\Lambda}\text{C}$ , three low-lying  $1^-$  states based on the  $3/2^-$  gs,  $1/2^-$  2.00 MeV and  $3/2^-$  4.80 MeV states of the  ${}^{11}\text{C}$  core can be formed in the  $(\pi^+, K^+)$  reaction. The upper two  $1^-$  states are relatively weakly formed with strengths that are very sensitive to small admixtures of the weak-coupling basis configurations. The  $p_{NS\Lambda}$  interaction favored by Millener et al.<sup>20</sup> shifts formation strength into the lowest  $1^-$  level ( ${}^{12}_{\Lambda}\text{C}$  ground state); the sensitivity of both excitation energies and formation strengths to the  $\Lambda N$  effective interaction is clearly evident in Table III of Ref. 20, as are the small doublet separations for the standard  $\Lambda N$  interaction.

## 2. Coincidence reactions

### (a) $(\pi^+, K^+\gamma)$ reactions

Hypernuclear  $\gamma$ -ray transitions in  ${}^7_{\Lambda}\text{Li}$  and  ${}^9_{\Lambda}\text{Be}$  have been observed with NaI detectors using the  $(K^-, \pi^-\gamma)$  reaction at Brookhaven.<sup>21</sup> Subsequently, attempts were made with Ge(Li) detectors to observe  $\gamma$ -ray transitions between the members of ground state doublets in  ${}^{10}_{\Lambda}\text{B}$  and  ${}^{16}_{\Lambda}\text{O}$ . These experiments proved to be very difficult and near the limit of experiments possible at the AGS. The non-observation of a transition from the  $2^-$  member of the ground state doublet in  ${}^{10}_{\Lambda}\text{B}$  to the  $1^-$  ground state suggests that the doublet splitting is considerably smaller than the predicted<sup>20</sup> 170 keV. For a sufficiently small separation, of the order of 100 keV, the  $2^-$  state will preferentially weak decay as the M1 partial lifetime becomes longer than  $\sim 200$  ps.

The  $(\pi^+, K^+\gamma)$  reaction could provide greater sensitivity to look for  $\gamma$  transitions between the members of ground state doublets. Also, it may be possible to utilize the

resolution of Ge(Li) detectors to look for higher energy transitions ( in the few MeV range) between the members of doublets based on different core states. In this way, it may be possible to measure doublet splittings indirectly and perhaps see several transitions in a  $\gamma$ -ray cascade. In some instances, the resolution of NaI detectors may suffice.

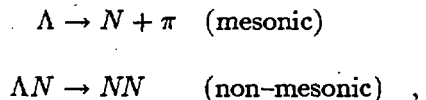
In many cases, hypernuclear states formed at high excitation energies will particle decay leading to the possibility of observing  $\gamma$  transitions in a daughter hypernucleus. For example, Majling et al.<sup>22</sup> have estimated the particle decay widths of hypernuclear states formed in  $(K^-, \pi^-)$  reactions and predicted the  $\gamma$ -ray lines that should be seen for specific cuts on the momentum of the outgoing pion (i.e. certain regions of excitation in the primary hypernucleus). Similar calculations could easily be made for primary hypernuclear production using the  $(\pi^+, K^+)$  reaction.

(b)  $(\pi^+, K^+)$  reactions

The spectra of the decay products from the breakup of an excited  $\Lambda$  hypernucleus formed in the  $(\pi^+, K^+)$  reaction carry useful information on the structure of the structure of the parent hypernuclear state. Majling et al.<sup>22</sup> have urged the measurement of both particle and  $\gamma$  spectra as tools to investigate hypernuclear structure.

(c) *Weak-decays of  $\Lambda$  hypernuclei*

The ultimate fate of a  $\Lambda$  hypernucleus is to weak decay via one or other of the two processes



with the non-mesonic mode dominating for all but the lightest systems. The decay can take place from the ground state or from an excited state whose electromagnetic lifetime is long compared with that for weak decay (typically  $\sim 200$  ps). Weak lifetimes have recently

been measured<sup>23</sup> for  ${}^{12}_{\Lambda}\text{C}$  and  ${}^{11}_{\Lambda}\text{B}$  ( $211 \pm 31$  and  $192 \pm 22$  ps. respectively) and lifetime measurements for heavier systems are desirable. Of even more interest, are measurements of the various partial decay rates such as the division into mesonic and non-mesonic and especially the ratio for proton stimulated to neutron stimulated non-mesonic decay. The ratio of  $\Gamma_{\Lambda n \rightarrow np}$  to  $\Gamma_{\Lambda n \rightarrow nn}$  is sensitive to the relative contribution of different meson exchanges in the  $\Lambda N \rightarrow NN$  weak decay process (see e.g. Ref. 24). Measurements of this ratio have been made<sup>25</sup> for the non-mesonic decays of  ${}^{12}_{\Lambda}\text{C}$  and  ${}^{11}_{\Lambda}\text{B}$ . but poor statistics lead to large errors on this very interesting quantity.

Measurements of the neutrons and protons which result from non-mesonic decay, and share the large energy release of  $176 - B_{\Lambda} - B_N$  MeV. for a range of light and a selection of medium and heavy nuclei would form a very interesting program. In many heavy nuclei, states involving the  $p_{\Lambda}$  orbit lie below the threshold for proton decay so advantage can be taken of the larger cross section for producing  $p_{\Lambda}$  states relative to  $S_{\Lambda}$  states (the produced hypernuclei then  $\gamma$  decay to the ground state).

Suggestions have also been made<sup>26</sup> to study the non-mesonic weak decay of  $p$ -shell  $\Lambda$  hypernuclei by looking at the delayed  $\gamma$ -rays from the  $A - 2$  daughter nuclei.

Recently, a very comprehensive study of the  $\pi$ -mesonic decay of  $p$ -shell  $\Lambda$  hypernuclei has been made.<sup>27</sup> The calculation includes  $\pi^0$  and  $\pi^-$  total mesonic decay rates, the partial decay excitation functions and pion angular distributions from polarized hypernuclei. The actual decay rates are very sensitive to details of the pion optical potential.<sup>27-29</sup> However, the ratio  $\Gamma_{\pi^0}/\Gamma_{\pi^-}$  for specific nuclear states are not. The  $\pi^0/\pi^-$  ratio can, in many cases, be used to distinguish the spin of the decaying member of a ground state doublet. The spectrum for decays to individual nuclear final states is generally an even more sensitive test of the spin of the initial hypernucleus and of hypernuclear structure.

(d) *Polarization of hypernuclei in the  $(\pi^+, K^+)$  reaction*

Bandō et al.<sup>30</sup> have calculated cross sections and polarizations for the  $(\pi^+, K^+)$  reaction on  $^{12}\text{C}$ ,  $^{16}\text{O}$ ,  $^{28}\text{Si}$ , and  $^{56}\text{Fe}$  targets using the elementary non-spin-flip  $f$  and spin-flip  $g$  amplitudes from a reanalysis of the  $\pi^- p \rightarrow K^0 \Lambda$  data. Large polarizations can be obtained for certain states which are populated with appreciable cross section; generally speaking the cross sections (for natural parity states) drop with increasing angle while the polarizations increase. E.g., the polarization for the  $^{12}_\Lambda\text{C } 1^-$  ground state reaches 50% at  $\theta \sim 15^\circ$  with a cross section of  $\sim 3 \mu\text{b/sr}$  at  $p_\pi = 1.04 \text{ GeV}/c$ .

The polarization is especially useful when combined with coincidence measurements of secondary decay particles, as in the weak decay examples discussed above.

### 3. Summary

Intense  $\pi^+$  beams and high resolution spectrometers would open up a very broad field of hypernuclear structure studies with the  $(\pi^+, K^+)$  reaction. The coincidence detection of hypernuclear decay products including  $\gamma$  rays would provide severe tests of the  $\Lambda N$  effective interactions used in hypernuclear structure models and of the models themselves. Information on the weak-decay properties of hypernuclei could provide strong constraints on the meson exchange mechanism for the non-mesonic  $\Lambda N \rightarrow NN$  decay mode. Observations of the mesonic decay mode would provide definitive information on hypernuclear structure and on pion distorted waves in the nuclear interior.

A large number of theoretical tools are at hand to interpret the experimental results. Detailed models of hypernuclear structure and the reaction mechanisms of hypernuclear production and decay have been developed and, in the absence of precise data, remain to be fully tested.

It will be interesting to see if a  $\Lambda NN$  three-body interaction<sup>31</sup> or a density-dependent two-body interaction,<sup>8</sup> which appear to be necessary to reproduce absolute binding energies of  $\Lambda$  hypernuclei, are necessary to reproduce the details of hypernuclear level schemes.  $G$ -matrices<sup>32</sup> obtained from the Nijmegen two-body potentials have some interesting characteristics which differ from the  $NN$  interaction. Bandō & Motoba<sup>2</sup> give as an example the repulsive pairing behavior for  $Nd_{5/2} \Lambda d_{5/2}$  configurations in which the  $4^+$  state lies 1 MeV below the  $0^+$  state in  ${}^{\Lambda}_{\Lambda}O$ ; the  $0^+$  state would be populated strongly by the  $(K^-, \pi^-)$  reaction and the  $4^+$  state by the  $(\pi^+, K^+)$  reaction, but it would require good resolution for both reactions to measure the  $0^+ - 4^+$  energy difference.

**Table 1.** Ground state ( $\pi^+$ ,  $K^+$ ) cross sections ( $\mu\text{b}/\text{sr}$ )

Angle	$^{28}\text{Si}$	$^{40}\text{Ca}$	$^{51}\text{V}$	$^{90}\text{Zr}$	$^{208}\text{Pb}^a$
$0^\circ$	3.7	1.4	3.5	2.0	0.55
$10^\circ$	1.8	0.5	1.4	0.8	0.15

$^a$   $i_{13}^{-1} s_A$

**Table 2.**  $^{89}\text{Y}(\pi^+, K^+)_{\Lambda}^{89}\text{Y}$  cross sections ( $\mu\text{b}/\text{sr}$ ) for pure particle-hole configurations (summed over  $\Lambda$  spin-orbit doublets).

Configuration	$\Delta L$	$0^\circ$	$5^\circ$	$10^\circ$	$15^\circ$	$20^\circ$
$g_{9/2}^{-1} s_{\Lambda}$	4	2.05	1.67	0.82	0.16	0.013
$g_{9/2}^{-1} p_{\Lambda}$	5	8.70	7.52	4.54	1.52	0.17
$g_{9/2}^{-1} d_{\Lambda}$	6	18.8	17.0	12.0	5.6	1.2
	4	2.1	1.5	0.47	0.15	0.18
$g_{9/2}^{-1} f_{\Lambda}$	7	27.1	25.3	19.6	11.2	3.81
	5	5.4	4.3	1.9	0.40	0.19
$g_{9/2}^{-1} g_{\Lambda}$	8	7.5	7.4	6.7	5.1	2.7
	6	15.9	13.8	8.6	3.2	0.53
	4	0.75	0.49	0.21	0.32	0.23
$f_{7/2}^{-1} s_{\Lambda}$	3	0.60	0.42	0.12	0.01	0.01
$f_{7/2}^{-1} p_{\Lambda}$	4	3.4	2.7	1.2	0.19	0.03
$f_{7/2}^{-1} d_{\Lambda}$	5	9.3	7.9	4.4	1.3	0.13
$f_{7/2}^{-1} f_{\Lambda}$	6	15.8	13.9	9.0	3.6	0.66
	4	0.84	0.57	0.17	0.12	0.12
$p_{3/2}^{-1} f_{\Lambda}$	4	0.14	0.38	0.89	0.95	0.35
$f_{5/2}^{-1} g_{\Lambda}$	7	18.7	17.5	13.7	8.0	0.13
	5	3.6	2.9	1.3	0.28	0.13

## FIGURE CAPTIONS

Fig. 1. Relative strength for transitions to states in  ${}^{56}\text{Fe}$  induced by the  $(K^-, \pi^-)$ ,  $(\pi^+, K^+)$  reaction on a  ${}^{56}\text{Fe}$  target. The strength is in units of  $N_{\text{max}}$ , the effective neutron number of the strongest transition. The selectivity of the  $(K^-, \pi^-)$  process at  $0^\circ$  in flight for low spin substitutional states and the tendency for the  $(\pi^+, K^+)$  reaction to populate a trajectory of high spin states ( $f_{7/2}^{-1} \times j_\Lambda$ ) is evident from the figure, which has been adapted from Bandō & Motoba;<sup>7</sup> the  $f_{7/2}^{-1}$  series is highlighted.

Fig. 2. The excitation spectrum for the  ${}^{89}\text{Y}(\pi^+, K^+){}^{89}\text{Y}$  reaction at 1.05 GeV/c and  $\theta_{K^+} = 10^\circ$ , from an AGS experiment.<sup>3-7</sup> The predicted  $\Lambda$  binding energies  $B_\Lambda$  for single particle configurations ( $g_{9/2}^{-1} \times \ell_\Lambda$ ) are indicated. The black dots below the ground state indicate the measured background.

Fig. 3. Data on binding energies of  $s$ ,  $p$ ,  $d$ ,  $f$  single particle states of the  $\Lambda$  as a function of  $A^{-2/3}$ , from Millener et al.<sup>6</sup> The curves correspond to a nonlocal  $\Lambda$ -nucleus potential with  $\rho^2$  density dependence, as explained in the text.

Fig. 4. The measured  $(K^-, \pi^-)$  and  $(\pi^+, K^+)$  excitation spectra on a  ${}^9\text{Be}$  target. The  $(K^-, \pi^-)$  forward angle data at 720 MeV/c are replotted from Bertini et al.<sup>13</sup> The  $(\pi^+, K^+)$  spectrum at 1.05 GeV/c,  $\theta = 0^\circ$ , has been obtained from P. Pile (private communication).

Fig. 5. The effective neutron number  $N_{\text{eff}}$  for the  $(K^-, \pi^-)$  and  $(\pi^+, K^+)$  reactions on  ${}^9\text{Be}$ , as calculated by Bandō.<sup>13</sup> The forward differential cross section for each hypernuclear state with binding energy  $B_\Lambda$  is given by  $N_{\text{eff}}(d\sigma/d\Omega)_{2\text{-body}}$  in terms of the  $K^-n \rightarrow \pi^-\Lambda$  or  $\pi^+n \rightarrow K^+\Lambda$  two-body  $0^\circ$  cross section  $(d\sigma/d\Omega)_{2\text{-body}}$ . The states in  ${}^9_\Lambda\text{Be}$  are labeled by orbital angular momentum  $L$  and parity  $\pi$ , in a coupling scheme where  $J = L + s_\Lambda$ . Thus, each line with  $L \neq 0$  corresponds to a doublet for which the spin splitting is neglected. Note the strong selectivity of both the  $(K^-, \pi^-)$  reaction, which has low  $q$  and favors  $\Delta L = 0$  transitions, and the  $(\pi^+, K^+)$  process, which has  $q \approx 350$  MeV/c and preferentially excites the higher spin  ${}^9_\Lambda\text{Be}$  states.

## REFERENCES

1. C. B. Dover, L. Ludeking and G. E. Walker, Phys. Rev. C22 (1980) 2073.
2. H. Bandō and T. Motoba, Prog. Theor. Phys. 76 (1986) 1321.
3. H. Bandō, Nucl. Phys. A478 (1988) 697c.
4. C. Milner et al., Phys. Rev. Lett. 54 (1985) 1237.
5. R. E. Chrien, Nucl. Phys. A478 (1988) 705c.
6. J. C. Peng, AIP Conference Proceedings, No. 176 (1988) 39.
7. P. H. Pile, in Proc. of V<sup>th</sup> Int. Conf. on *Clustering Aspects in Nuclear and Subnuclear Physics*, Kyoto, Japan (1988), to be published.
8. D. J. Millener, C. B. Dover and A. Gal, Phys. Rev. C38 (1988) 2700.
9. Y. Yamamoto, H. Bandō and J. Zofka, Prog. Theor. Phys. 80 (1988) 757.
10. R. H. Dalitz and A. Gal, Ann. Phys. (NY) 131 (1981) 314.
11. E. H. Auerbach et al., Ann. Phys. (NY) 148 (1983) 381.
12. T. Yamada, K. Ikeda, H. Bandō and T. Motoba, Phys. Rev. C38 (1988) 854.
13. R. Bertini et al., Phys. Lett. 90B (1980) 375.
14. T. Motoba, Nucl. Phys. A479 (1988) 227c.
15. T. Motoba, H. Bandō, R. Wünsch and J. Zofka, Phys. Rev. C38 (1988) 1322.
16. T. Motoba, in *International Symposium on Hypernuclear and low-energy Kaon Physics*. Padova (1988).
17. R. Hausmann and W. Weise, Nucl. Phys. A491 (1989) 598.
18. R. K. Jolly and E. Kashy, Phys. Rev. C4 (1971) 1398;  
A. Chaumeaux et al., Nucl. Phys. A164 (1971) 176;  
S. Sen et al., Phys. Rev. C6 (1972) 2201.
19. R. H. Dalitz, D. H. Davis and D. N. Tovee, Nucl. Phys. A450 (1986) 311c.
20. D. J. Millener, A. Gal, C. B. Dover and R. H. Dalitz, Phys. Rev. C31 (1985) 499.
21. M. May et al., Phys. Rev. Lett. 51 (1983) 2085.
22. L. Majling et al., Nucl. Phys. A450 (1986) 189c; Phys. Lett. 130B (1983) 235; Phys. Lett. 183B (1987) 263.

23. R. Grace et al., Phys. Rev. Lett. 55 (1985) 1055.
24. J. F. Dubach, Nucl. Phys. A450 (1986) 71c.
25. J. J. Szymanski, A.I.P. conf. proc. 150 (1986) 934.
26. L. Majling et al., Phys. Lett. 202B (1988) 489.
27. T. Motoba, K. Itonaga and H. Bandō, Nucl. Phys. A489 (1988) 683.
28. K. Itonaga, T. Motoba and H. Bandō, Z. Phys. A330 (1988) 209.
29. R. Mach et al., Z. Phys. A331 (1988) 89.
30. H. Bandō, T. Motoba, M. Sotona and J. Zofka, Fukui University preprint, FUMP-1988-8.
31. A. R. Bodmer and Q. N. Usmani, Nucl. Phys. A477 (1988) 621.
32. Y. Yamamoto and H. Bandō, Prog. Theor. Phys. Suppl. No. 81 (1985) 9.